Journal of
Synchrotron Radiation

ISSN 0909-0495

Received 1 March 2009
Accepted 24 July 2009

Experimental observation of a strange temporal oscillation of X-ray Pendellösung fringes

Jun-ichi Yoshimura* and Keiichi Hirano

Photon Factory, Institute of Materials Structure Science, High Energy Accelerator Research Organization, 1-1 Oho, Tsukuba, Ibaraki 305-0801, Japan. E-mail: jun-ichi.yoshimura@kek.jp

As a strange property not explained by existing theories, it has been known from experiment that X-ray moiré and Pendellösung interference fringes show a small spatial oscillation in the beam path in free space that the diffraction image carrying those fringes is propagated after emerging from the crystal. In connection with the investigation into this strange fringe oscillation, it has been found, by an experiment successively recording Pendellösung-fringe topographs using an X-ray CCD camera, that X-ray Pendellösung fringes also show a small temporal oscillation. Characteristics of this temporal Pendellösung-fringe oscillation, namely irregularities in the fringe profile, the manner of fringe oscillation and a reciprocal correlation between oscillation amplitude and fringe contrast, are shown to be very similar to those of the previously reported spatial oscillation of moiré and Pendellösung fringes. Therefore this temporal oscillation is supposed to have the same origin as the spatial oscillation, revealing another section of the same phenomenon. This discovery of the temporal oscillation advances a step nearer to the full understanding of this strange phenomenon, while disclosing a new property of Pendellösung fringes. As well as the above, a three-dimensional profile representation (surface plot) is given of the image of Pendellösung fringes, to make it clear that unidentified fine intensity modulations, called subfringes in this paper, are produced superposed on the main fringe system. Overall inspection of the intensity profiles of the fringe-imaged topographs suggests that temporal intensity oscillations also occur on a more global scale than the extension of individual fringes, as an unidentified action of the wavefield.

Keywords: X-ray interferometry; Pendellösung fringes; fringe profile analysis; temporal fringe oscillation; surface-plot analysis; X-ray CCD camera.

1. Introduction

It has been known from experiment that X-ray moiré and Pendellösung interference fringes show a strange spatial oscillation in the beam path in free space that the diffraction image carrying those fringes is propagated after emerging from the crystal (Yoshimura, 1989, 1991, 1993, 1996, 2000). This strange fringe oscillation is generally observed in X-ray diffraction experiments using a well collimated beam, irrespective of the type of X-ray source (laboratory source or synchrotron radiation), and, for moiré fringes, irrespective also of the type of moiré pattern (rotation moiré or parallel moiré) and of how they are created (by bi-crystal or by LLL interferometer). Therefore this fringe oscillation is suggested to be a general property of these interference fringes. The fringe oscillation remains theoretically unexplained up to now. Since it is an irregular oscillation occurring as an oscillatory change of irregular asymmetric-shaped fringe profiles, it does not seem to be readily derived or explained from another known interference phenomenon. The authors, on the contrary, suppose that this is quite a new phenomenon touching the innermost nature of X-ray interference and probably of the interference of light waves.

For such a spatial fringe oscillation, the question is naturally raised as to whether or not a corresponding temporal fringe oscillation also occurs. To investigate this question, the authors performed an experiment several years ago recording successively a Pendellösung-fringe image onto moving X-ray films, and obtained a result which seems to show the occurrence of a temporal fringe oscillation (Kanamori *et al.*, 2000). However, it was difficult at that time to verify whether the successive imaging positions (namely the crystal-to-film distance) were identical, and therefore a definite claim for the observation of the temporal oscillation was not made. This time we again performed an experiment investigating the occurrence of the Pendellösung-fringe temporal oscillation using an X-ray CCD camera, and obtained a result showing the expected temporal oscillation. The imaging position of

successively recorded data images (with a time interval not shorter than 0.66 s) on the CCD camera which was fixed in position is exactly the same, and an oscillatory change seen among the data images is certainly understood to show a temporal oscillation of the fringes. This discovery of the Pendellösung-fringe temporal oscillation adds new information to the study of the strange fringe oscillation mentioned, and revises our knowledge of Pendellösung fringes.

2. Experimental procedure

The experiment was conducted using synchrotron radiation at station BL-15C at KEK-PF, Japan, using the set-up illustrated in Fig. 1. X-rays from the synchrotron source were monochromated and collimated by a Si 111 double-crystal premonochromator set and another double-crystal arrangement (parallel setting) of Si 220 collimators whose surfaces are asymmetrically cut to 10.0° and 10.1° off the (110) plane, respectively (the asymmetry factors are estimated to be b = 0.10 and b = 0.096, respectively, at the wavelength used). The wavelength of the incident X-rays onto the specimen was centred at $\lambda_0 = 0.81$ Å (15.3 keV) with a spread of $\Delta\lambda/\lambda_0 = 4.3 \times 10^{-4}$. The angular spread was 0.034″ for individual wavelengths, and 0.079″ over the entire wavelength range. Specimens were wedge crystals as illustrated in Fig. 1(*b*), which gave fringe spacings of 0.275, 0.345 and 0.463 mm for the wavelength and the reflection used. All the specimens were cut from a FZ silicon block. The 220 reflection was used in the symmetric Laue geometry, the specimen being set in a parallel setting with the upstream Si 220 collimator (C2). The Bragg angle for the 220 reflection is $\theta_B = 12.2°$.

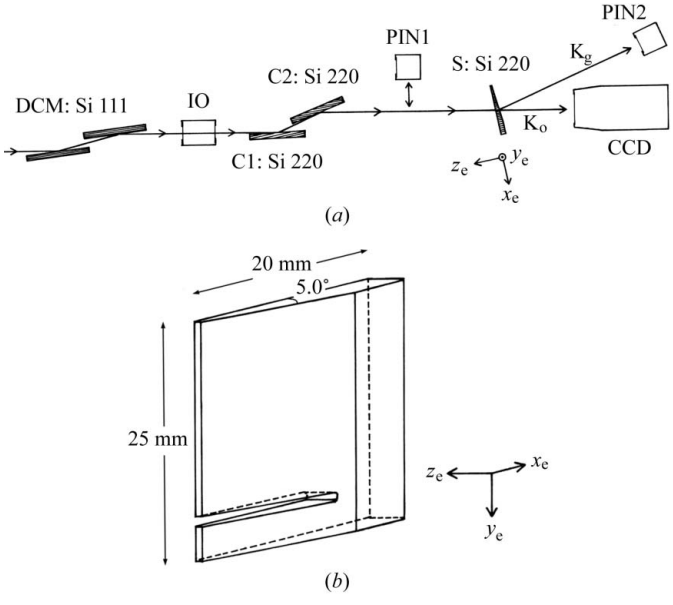

Figure 1
(*a*) Experimental set-up. DCM: double-crystal premonochromator set upstream of the experimental hutch. IO: ionization chamber. C1 and C2: parallel double-crystal setting of asymmetric-cut crystals of silicon. PIN1 and PIN2: PIN detectors. S: specimen crystal. CCD: X-ray CCD camera. x_e axis parallel to [110], y_e axis parallel to [$\bar{1}$10], z_e axis parallel to [001]. The x_e and z_e axes are in the vertical plane. (*b*) Detailed drawing of the specimen wedge crystal. The wedge angle 5.0° is for the fringe spacing of 0.345 mm.

Twenty pictures of the forward-diffracted image (*O* image) of the specimen wedge crystal in which an equal-thickness Pendellösung fringe pattern is produced were successively recorded on an X-ray CCD camera placed about 30 cm behind the specimen, with a time interval of 0.66–4.3 s. The corresponding net exposure time was 0.5–4.0 s. The intensity of the diffracted beam monitored during the imaging run (by PIN2 in Fig. 1) was completely unchanged or very slightly changed (zero to a few tenths percent). The main data images including those presented in this paper were recorded at the peak position of diffracted intensity. The X-ray CCD camera used was a Photonic Science XFDI 40 mm (resolution 24.0 µm), and was operated in the 12-bit mode at 10 MHz speed, with gain = 1 and dark field subtraction disabled. All the data images were overviewed; after this overall inspection, in this paper we describe the result of imaging with a 2.3 s interval (net exposure time 2.0 s) for the specimen with 0.345 mm fringe spacing. Images recorded by the fastest imaging, *i.e.* with a 0.66 s interval, taken with 2 × 2 binning, were insufficient in terms of spatial resolution, and were deemed not good enough for use as main data. Besides the CCD imaging above, a Pendellösung-fringed image was also recorded simultaneously onto multi-stacked X-ray films (Fuji #50) for reference, as in the previous experiments (*e.g.* Yoshimura, 2000). The exposure time was 40 s. Double-coated films were used as received, unlike in the previous experiments, and only one side of them was developed in post-processing. The photographic density on the films was read into a computer by a film scanner [Nikon, Coolscan V ED (14-bit levels, 4000 dpi)]. *Image J* (version 1.38) was used as the main software in the processing and analysis of the acquired CCD and film data.

3. Results

3.1. Pendellösung fringes in topographic images

Fig. 2 shows an overall view of one of the 20 successively recorded Pendellösung-fringe topographs. As describe earlier, this is a forward-diffracted image (*O* image), and the fringe spacing is 0.345 mm, disregarding the fringe oscillation under study. The sense of image contrast is such that white contrast indicates higher intensity, as in the previous studies. Fringes are numbered from left to right as fringe 1, fringe 2 *etc.* up to fringe 36. The coordinate system (*X*, *Y*) in the image plane of the topographs is taken as indicated in the figure. In the image analysis the line profile was measured along the *X* axis at several *Y* positions around *Y* = 10.0 mm. As observed, there is no extended strain in the topograph. Observed defect-like images (noted by oblique arrows) all come from the upstream monochro-collimator crystals. Although ideally the image intensity should be perfectly uniform in the vertical direction, a very weak non-uniformity is present in the vertical direction owing to a slight misadjustment of the tilt angle.

Fig. 3 compares the first four topographs of successive imaging in a small field where low-contrast fringes are present.

Smoothing was not performed on these topographs [however, the picture size was adjusted using *Photoshop* (version 7) using the nearest-neighbour method]. Although the image resolution is not very high, it can be seen that the detail in the fringe pattern changes among the member topographs of the set of 20. The fringe direction, fringe spacing and profile width of the fringes *etc.* change on a local scale. For example, the letters B, D, E and I show (below the labels) a small local bending of the fringes, G and H show a local broadening or narrowing of the fringe spacing (compared with other topographs), and F shows a 'contact' or 'coalescence' of adjacent fringes. Letters A and C show the presence of fine striations crossing the main Pendellösung fringes, though these are very weak signals (see §3.5.1). The lower images in Fig. 3 are double-size enlargements of the lower-right-hand quarter of the corresponding upper images, showing more clearly that the fringe pattern changes among the topographs. Pixel-sized dots of white or black contrast scattering in the topographs could be attributed to detector noise. The discussion of fringe motion here is not free from the consideration of noise. However, the changes in the fringe pattern mentioned are considered to be basically real, not created by noise, since a correlated intensity change over dozens of pixels would be necessary to produce such changes. Although the fringe pattern changes mentioned could incorrectly be disregarded for the reason that they are small, irregular and local, they should never be neglected from a theoretical viewpoint expecting exactly regular-profiled fringes at rest (*e.g.* Kato, 1974).

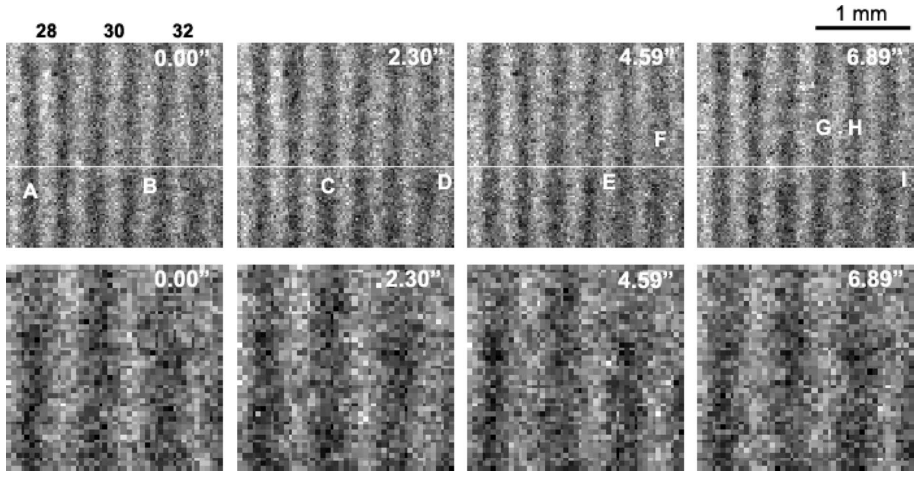

Figure 3
Upper images: comparison of the first four topographs of successive imaging. Numbers in the upper-right in each topograph give the recorded time. Numbers at the top of the 0.00″ topograph give the fringe number. Horizontal lines are drawn at Y = 10.0 mm. For letters A, B, *etc.* and the four lower images, see text.

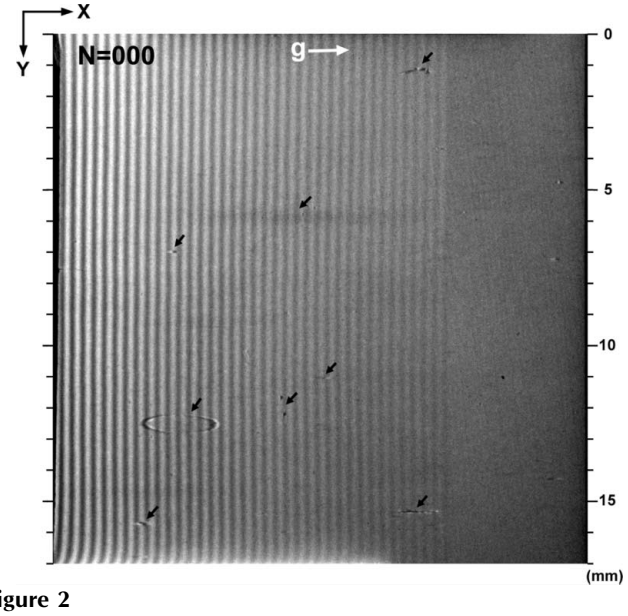

Figure 2
Overall view of the Pendellösung-fringe topograph studied (the first of all 20 topographs). *O*-beam image. **g** is the diffraction vector. Oblique arrows mark defect or blur images coming from the upstream monochro-collimator crystals.

3.2. Fringe profiles

Fig. 4 shows an example of fringe profiles measured in the first ten topographs of the 20 successively recorded ones, along the X axis at Y = 10.0 mm (see Figs. 2 and 3). This line-scan analysis was made on unsmoothed data images as recorded by the CCD camera, with a line width of three pixels (0.072 mm). The numbers in the upper right in each graph give the recorded time of imaging. Remarks on the fringe profiles are as follows.

3.2.1. Overall observation. (i) It should first be pointed out that the fringe profiles (on the right-hand-side graphs) are generally irregular- and asymmetric-shaped with a subpeak structure in some fringes, whereas theoretical calculation predicts profiles of regular, almost sinusoidal, shape [see Fig. 4 of Yoshimura (2000)]. The question concerning the influence of detector noise will be discussed in §3.2.2 and §3.5.1.

(ii) Among the member topographs with different recorded times, fringes repeat an oscillatory or a roughly periodical change in various elements of the fringe profile. For example, fringes 28, 30 *etc.* show an obvious alternating change in shape asymmetry, showing a to-and-fro head-shaking. In a typical way the profile inclines to one side with its top shifted in the same direction, while its bottom positions are displaced in the opposite direction (see fringe 28 from 11.49″ to 13.78″). In fringes 26, 28 *etc.* the profile height shows an oscillatory change with appreciable magnitude, and in fringes 23, 31, 33 *etc.* the width of the profile changes in an oscillatory way. The motion of these profile changes is never confined to the ten topographs shown, but continues to the 20th topographs (43.64″). While the profile change is mentioned, it should also be noted that there are some fringes which show only a small change throughout the 20 topographs (see fringes 22, 24 *etc.*).

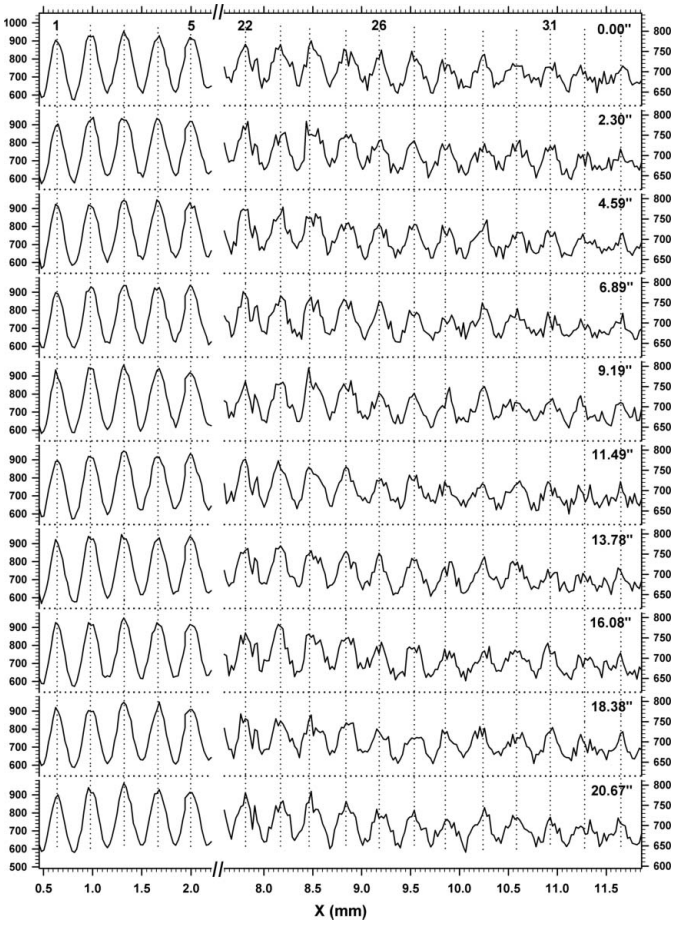

Figure 4
Comparison of intensity profiles of the first ten Pendellösung-fringe topographs of all 20 successively imaged, scanned along the X axis at a height of Y = 10.0 mm with a 3-pixel line-width. The intensity shown (ordinate axis) is as recorded by the CCD camera with no processing. Numbers at the top of the figure denote the fringe number. Numbers in the upper-right in the graphs give the recorded time of the relevant topographs. The left-hand-side ordinate scale refers to the left-hand-side graphs, and the right-hand-side ordinate scale to the right-hand-side graphs.

(iii) In high-contrast fringes (the left-hand-side graphs), the profiles are almost well shaped in accord with the current theory and their peaks do not show a conspicuous change, in contrast to low-contrast fringes. However, it should be mentioned that a small oscillation also occurs very close to the profile top, in the profile shape and in the top position. Although the question of noise cannot be cleared out, the authors think this small change is basically real from an observation of many examples. The characteristics of the profile change described in (i), (ii) and (iii) all are similar to the previous observation of spatially oscillating moiré and Pendellösung fringes.

(iv) However, a minor difference from the previous Pendellösung fringes is that the profile-height and profile-width changes are comparatively small and moderate in the present profiles. In the previous paper, Yoshimura (2000) describes low and high levels of fringe oscillation; in the low level the oscillation occurs mainly through the shape-asymmetry change and bottom-position displacement, while in the high level changes in the peak height, profile width and subpeak structure become markedly large. In reference to this description the present fringe oscillation is at a rather low level even in the low-contrast region.

3.2.2. Detailed inspection of profile change. Before advancing to the next discussion, we should view the influence of detector noise on the fringe oscillation observation. If we presuppose that the fringed image under study is in motion, the magnitude of noise is understood to be that of the intensity fluctuation attributable to noise, included in each data image. To obtain this noise-attributable intensity fluctuation, we recorded the incident intensity with the CCD camera at various intensity levels and analyzed it in the same way as the data images were acquired and analyzed. Twenty multiple images were successively recorded with a 2.0 s exposure time, and line-scan analysis with a 3-pixel line-width was carried out. Here the incident intensity means the diffracted intensity from the C2 collimator and that from the Si 111 DCM (see Fig. 1). The results of the analysis for the two diffracted intensities agreed satisfactorily with each other. The incident intensity is ideally considered to be temporally constant. From this measurement and analysis, we obtained an empirical equation for the incident intensity standard deviation $\sigma_{\rm I}$,

$$\sigma_{\rm I}(\bar{I}) = -0.70 + 0.27\,\bar{I}^{\,0.564} \qquad (0 \le \bar{I} \le 2000). \qquad (1)$$

Here $\bar{I}$ is the mean intensity over the 20 recorded images. For $\bar{I}$ = 700, $\sigma_{\rm I}$ = 10.2 $\pm$ 1.5. For the moment we should accept this as the measure of detector noise.

With this noise estimation taken into consideration, we show a detailed comparison of the fringe profiles in Fig. 5. The letters A and B in the first graph indicate the changes in profile height as mentioned in §3.2.1. Letters B, C, D, F, H and I indicate the mentioned shape-asymmetry changes and accompanying displacements of the top and bottom positions of the profiles. The letter E shows an example of profiles which show a considerably large displacement as a whole, and letter G indicates the mentioned change in profile width. When the error bar range is taken to be $\pm\sigma_{\rm I}$, as shown in the graphs, the mentioned profile changes could be approved in the mass. However, when we take the error bar range as $\pm 1.96\sigma_{\rm I}$, the confidence intervals of mutually compared profiles do not separate from each other in almost all profiles. Thus, the reliability of the claim for the fringe-profile change is not assessed to be high enough from the viewpoint of general statistics. Nevertheless, the mentioned profile changes are all considered to be basically real for similar reasons as described in §3.1. Single noise pulses scattering homogeneously cannot produce such a sizeable change of pattern. Fringe profiles, however, would not be affected a little by noise. Ripples and pointed peaks of profiles suggest the effect of noise.

Graph (*d*) plots the maximum and minimum intensities in the 20 data images presently discussed, measured from the mean intensity $\bar{I}$. The $\pm 1.96\sigma_{\rm I}(\bar{I})$ lines are drawn for reference. The number of data points, *i.e.* intensities, which are distributed outside the range $\pm 1.96\sigma_{\rm I}(\bar{I})$ is also plotted (plots at the middle height of the graph). Graph (*e*) shows the same plots as graph (*d*) but for the whole fringed region. The statistics of the

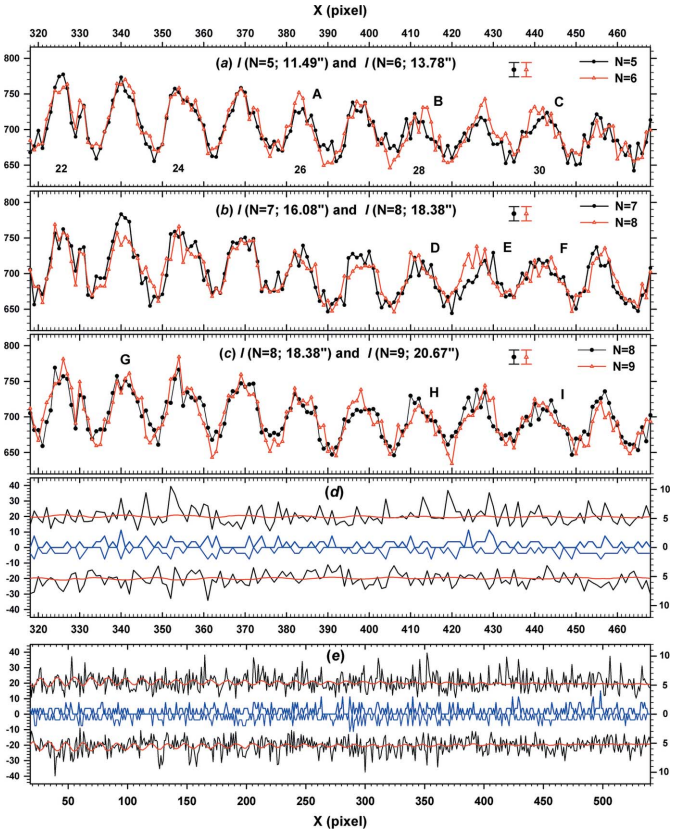

Figure 5
(*a*)–(*c*) Detailed comparison for part of intensity profiles given in Fig. 4. (*d*)–(*e*) Plots showing the statistical characteristics of intensity variation in the 20 data images. Numbers at the bottom of graph (*a*) give the fringe number. In graphs (*d*) and (*e*), plots are given from top to bottom as follows: the maximum intensity measured from the mean intensity ($I_{\max} - \bar{I}$), the line of $1.96\sigma_{\rm I}(\bar{I})$, the number n_+ of data points which are above $1.96\sigma_{\rm I}(\bar{I})$, the number n_- of data points which are below $-1.96\sigma_{\rm I}(\bar{I})$, the line of $-1.96\sigma_{\rm I}(\bar{I})$, and the minimum intensity ($I_{\min} - \bar{I}$). The numbers n_+ and n_- refer to the right-hand-side ordinate axis. For other features, see text.

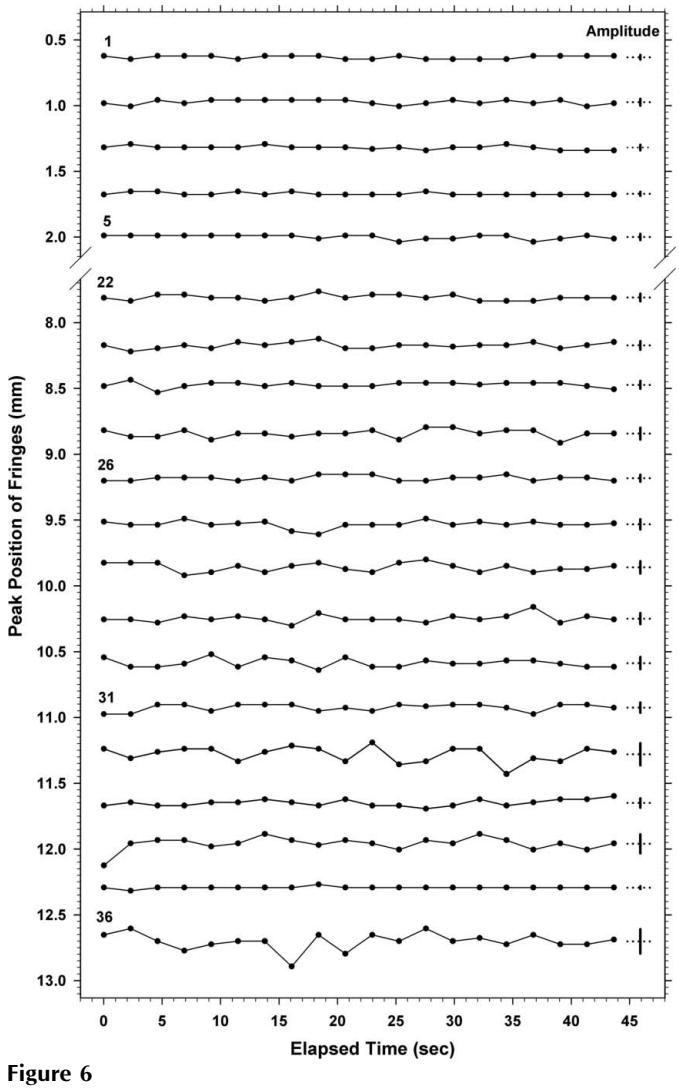

Figure 6
Plot of the top position of fringe profiles *versus* recorded time, determined from fringe profiles as given in Fig. 4. Numbers near the left-hand edge denote the fringe number. Vertical bars near the right-hand-side edge give the oscillation amplitude (see text).

two graphs are such that the variation in the data image intensity slightly exceeds the normal fluctuation level of noise in the incident intensity.

3.3. Fringe position plot and amplitude map of fringe oscillation

Fig. 6 shows a plot of fringe-peak position along the X axis *versus* observed time (recorded time), determined from fringe profiles in the multi-frame topographs as shown in Fig. 4. In this plot we have an overall view of the fringe oscillation in all 20 topographs. As in the previous papers (Yoshimura, 1996, 2000), analysis to determine the fringe position was carried out by defining the mid-position in profiles at 0.85 times the profile height measured from the bottom. However, we presently think that a plot of the non-averaged profile-top position better represents the characteristics of the fringe oscillation, although it is more easily subject to accidental disturbances of noise. For this reason the top-position plot is presented instead of the plot of 0.85-times-profile-height position. It should also be added that oscillations in the profile height and in the profile width are unjustly not taken into account in this oscillation evaluation. Vertical thick bars drawn near the right-hand-side edge indicate the mean oscillation amplitude for the respective fringes. The amplitude $a_{\rm P}$ was determined by the formula $a_{\rm P} = 2^{1/2}\sigma_{\rm P}$, with $\sigma_{\rm P}$ being the standard deviation in the position plot.

As shown in this graph, the present fringe oscillation is irregular in amplitude and in frequency. It is unknown whether the irregularity is essential to this fringe oscillation or not. This characteristic is also similar to the previous spatially oscillating fringes. It should be noted that, in addition to the general tendency that fringe oscillation is amplified with advance from high- to low-contrast fringes, the amplitude also changes on a more local scale. For example, in fringe 35, though its profiles are not shown in Fig. 4, the top position almost does not change its location in spite of having greatly oscillating adjacent fringes on both sides. It should also be remarked that a

very small oscillation seems to occur even for high-contrast fringes (fringes 1–5) with a meaningful profile change, not being due to noise. The oscillation amplitude in this plot was less than 1 pixel in the minimum, and more than 3.5 pixels in the maximum (24% of the mean fringe distance). This maximum amplitude is reduced to 2.5 pixels (17% of the mean fringe distance) in the 0.85-times-profile-height oscillation. The oscillation amplitude is appreciably lower than that of the previous Pendellösung fringes (33–38% of fringe spacing in the maximum; Yoshimura, 2004).

Fig. 7 shows the distribution of fringe oscillation amplitude over the entire fringe-imaged region, along with that of fringe contrast. As well as the oscillation amplitude in the top-position plot as given in Fig. 6, oscillation amplitudes in the bottom position of fringes and in the 0.85-times-profile-height position are given. The oscillation in the bottom position should be noted as well as the top-position oscillation. In fact, the oscillation amplitude in the bottom position is at about the same level as that in the top position on the whole. Furthermore, there seems to be a general tendency for the bottom-position oscillation to be large where the top-position oscillation is small, and *vice versa*. Fig. 7(*a*) further illustrates an approximate relationship between the amplitudes of the top-position oscillation and of the 0.85-times-profile-height oscillation. In the latter, small top-position oscillations in high-contrast fringes tend to be neglected, whereas regularity of this apparently irregular oscillation seems to be glimpsed in the small-oscillation region.

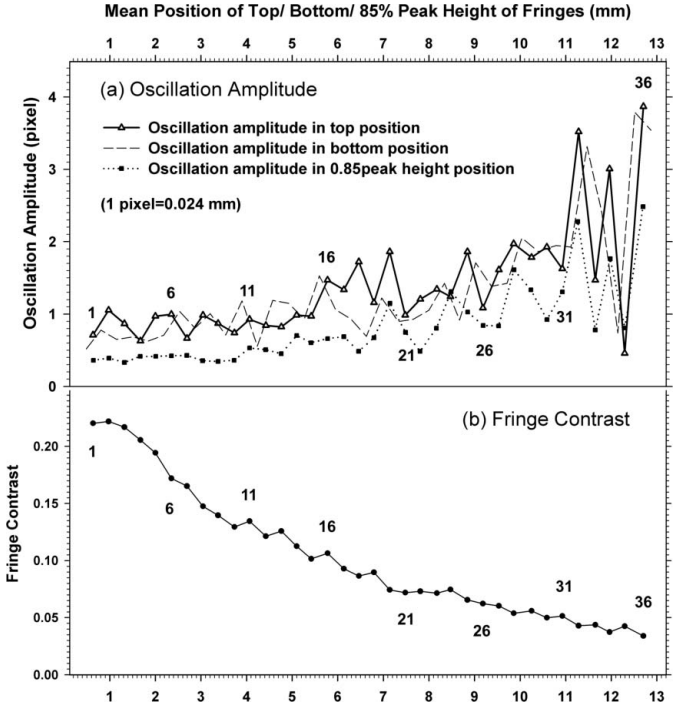

Figure 7
Fringe-by-fringe plots of (*a*) oscillation amplitudes and (*b*) fringe contrast. The oscillation amplitudes in different definitions are all derived from fringe profiles at $Y = 10.0$ mm, as given in Fig. 4. The fringe contrast is given as the mean value over all 20 topographs.

Comparison of the oscillation amplitudes (Fig. 7*a*) and the fringe contrast (Fig. 7*b*) shows that a relationship exists between the two. Qualitatively, a reciprocal correlation similar to the previous spatial fringe oscillation is also seen in this case. Quantitatively, the relationship obtained from fitting curves to the plot of oscillation amplitude *versus* fringe contrast (not shown here) was $a_P/L = 3.6 \times 10^{-5}V^{-2.6} + 0.062$ for the top-position oscillation, and $a_P'/L = 4.3 \times 10^{-4}V^{-1.7} + 0.021$ for the 0.85-times-peak-height oscillation. Here L denotes the mean fringe spacing and V the fringe contrast. The relationship for the previous Pendellösung fringes was $a_P'/L = 0.0075V^{-1.1} + 0.013$ (Yoshimura, 2004). Such a reciprocal correlation may be remarked as the first law on the present fringe oscillation. It should furthermore be noted that the oscillation amplitude shows a local oscillatory change in the top-position oscillation of the left ten or so fringes (Fig. 7*a*). As exemplified by this, the oscillation amplitude also seems to follow a minor second regulation on a local scale. A similar feature has been pointed out in a previous paper (Yoshimura, 2004). The repeat of maximum and minimum oscillations in several of the right-hand-side fringes (fringes 32–36) also suggests an operation of some controlling mechanism.

3.4. Fringe oscillation in multi-stacked-films images

Fig. 8 shows fringe profiles measured in Pendellösung-fringe topographs (*O* image) taken by simultaneous recording onto multi-stacked X-ray films, as in the previous experiments. The same specimen as dealt with in §3.1–§3.3 was imaged under the same experimental conditions using the same set-up (the fringe position is only slightly displaced from the case of Figs. 2–7). Numbers in the upper-right in each graph give the relevant specimen-to-film distance (in mm) along the beam path. Orienting and positioning the topographs and determination of the specimen-to-film distance were carried out with the aid of sharp scratch images in the topographs of forward-diffracted and diffracted images. The accuracy of positioning is estimated to be ± 1 pixel (6.35 μm) at 4000 dpi resolution. The intensity level (photographic density), which differs considerably with the topographs, was regulated to be much the same as each other in image processing. In Fig. 8, fringe-profile change and related fringe-peak oscillation are observed similarly to the previous fringes and to the fringe profiles in Figs. 4 and 5 of this paper (see, for example, fringes 25–27, 32, 33 *etc.*). The thick horizontal bars at the bottom indicate the oscillation amplitude of respective fringes (top-position oscillation), which is of magnitude 4–21% of the mean fringe spacing. It has thus been confirmed that a spatial fringe oscillation occurs in the same system as that where the temporal oscillation was observed.

3.5. Other related anomalies

Finally, it must be stated that anomalies of the present Pendellösung fringes are not confined to irregular-shaped profiles and oscillation of individual fringes. As examples of such as yet unmarked anomalies, we describe here fine subsidiary fringes and a global intensity oscillation.

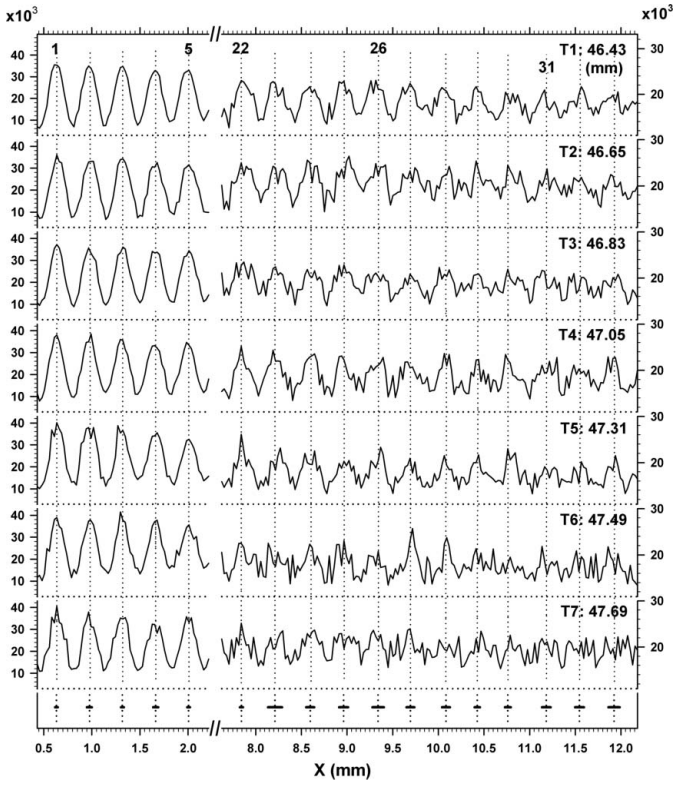

Figure 8
Intensity profiles of topographs recorded on multi-stacked films of simultaneous imaging, scanned along the X axis at a height of Y = 10.0 mm with line width of 0.0762 mm (3 pixels in 1000 dpi pictures). Smoothing was not carried out. The intensity scale in the $T1$ graph (top) is as read by the film scanner. The intensities in other graphs are arbitrarily corrected so that the intensity level of the profiles becomes much the same as that in $T1$. The left-hand-side ordinate scale refers to the left-hand part of the graph, and the right-hand-side ordinate scale to the right-hand part. For other features, see text.

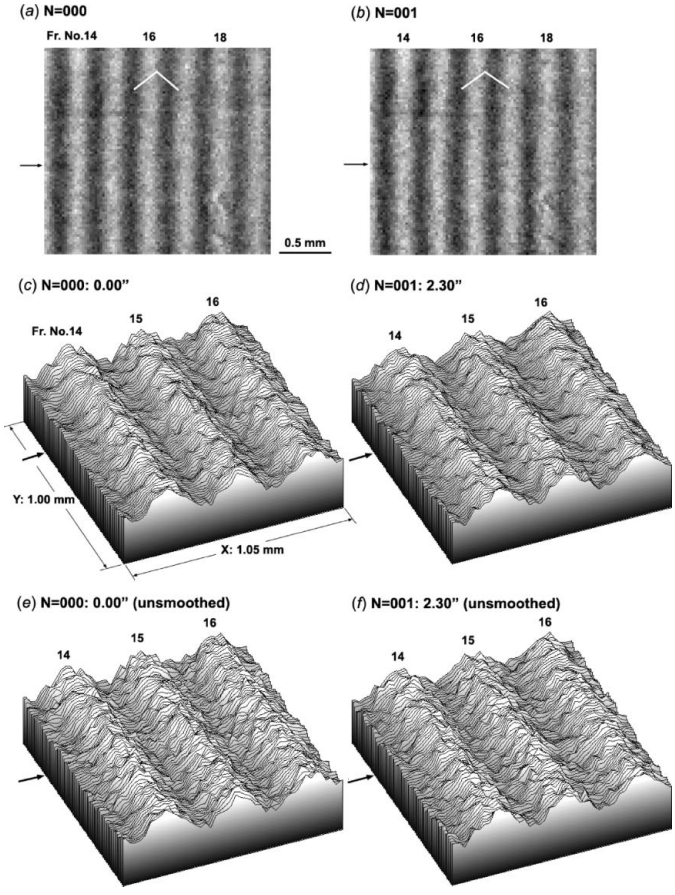

Figure 9
Usual-type topographs (a, b) and their three-dimensional profiles [surface plots; (c)–(f)] revealing subfringes superposed on main Pendellösung fringes. Arrows indicate the approximate position of Y = 10.0 mm. For further information, see text.

3.5.1. Fine subsidiary fringes. In X-ray topographs of moiré and Pendellösung fringes recorded with a well collimated beam, fine striations of faint contrast are generally observed to be superposed on the main fringe pattern, especially in their low-contrast region (Yoshimura, 1993; Yoshimura *et al.*, 2001). The authors have called them fine subsidiary fringes (hereafter subfringes). Such subfringes can be seen rather clearly in the original photographs, but it has been difficult to clearly reproduce them in printed matter. We now attempt to present such topographs (CCD images) showing subfringes in Figs. 9(a) and 9(b). If carefully observed, many subfringes can be seen to run in directions indicated by the white lines. Figs. 9(c) and 9(d) show the surface plot (hereafter called three-dimensional profiles) for the topographs (a) and (b), respectively, in their lower-left quarter. [In these three-dimensional profiles the intensity axis (vertical) is intentionally reduced so as not to create a blind spot.] Fine intensity modulations on the main Pendellösung fringes in the three-dimensional profiles correspond to subfringes in the topographs. This correspondence is confirmed, though is not clear in this presentation. (However, while subfringes running from the upper-left to the lower-right in the topographs are well represented in the three-dimensional profiles, those from the lower-left to the upper-right are not.) The presence of subfringes on the Pendellösung fringe pattern was thus able to be shown clearly using the 'Surface Plot' command of *Image J* (polygon multiplier 100%).

Figs. 9(e) and 9(f) show three-dimensional profiles of the same topographs made with the 'Smooth' function disabled, while the three-dimensional profiles in Figs. 9(c) and 9(d) were made with the smoothing enabled. Single sharp peaks in places in Figs. 9(e) and 9(f) are due to noise. These unsmoothed three-dimensional profiles give an idea as to what extent the fringe pattern is affected by noise. From observation and from comparison with the smoothed three-dimensional profiles, it may be affirmed that the fine modulation pattern of subfringes is basically not due to noise. The deformed shapes of the main fringe profile and their change may also be affirmed not to be due to noise.

In the case of the example shown, the intensity oscillation amplitude of subfringes was typically 30–60 (from bottom to top) on the main-fringe profile at an intensity of 650–850, expressed in 12-bit grey levels of the CCD camera. This was known by intensity scan along the main-fringe direction in the data image. The spacing of subfringes is roughly a few tenths of the main-fringe spacing, and the running direction is basi-

cally along two directions at roughly 50° from the main-fringe direction (see Figs. 9*a* and 9*b*). As described, they are quite common in moiré- and Pendellösung-fringe topographs with well collimated beam, and therefore are suggested to be an essential attendant of main fringes. Although we have tentatively called them subfringes from topographic observation, the three-dimensional profile observation gives a slightly different idea that they could be something like a wrinkle in the wavefield, caused by some instability. In this study, subfringes were found to be produced even on the highest-contrast main fringes (∼22% contrast). Subfringes are produced in a rather regular form in the high-contrast region, but with the decrease in main-fringe contrast they gradually become stronger-contrasted and form a disturbed pattern. This dependence on the main-fringe contrast is similar to that of fringe oscillation in main fringes. Subfringes also change among member topographs (see Figs. 9*c* and 9*d*). This change is more rapid and greater than that in the main fringes. From the characteristics described, the change in subfringes and that in the main fringes are supposed to be closely connected. Incidentally, by this three-dimensional profile observation it is made clear that subfringes are connected to the occurrence of undulations and subpeaks in main fringe profiles, although these irregularities could be connected with noise on the other hand. We have to revise the previous idea of Pendellösung fringes (and of moiré fringes, though not shown here) in that they are accompanied by such subfringes as an essential property.

3.5.2. Global intensity oscillation. The upper four graphs in Fig. 10 show the overall view of the intensity profiles of the fringed region in some of the member topographs. As demonstrated by these graphs, the imaginary baseline connecting the bottom positions of fringes oscillates with the topographs. Though less noticeable, the imaginary line connecting the tops of fringes also oscillates. Although it is not very easy to represent such oscillations distinctly in a limited-sized graph, an up-and-down motion of the baseline noted by the upward arrow can be seen with clarity. Though less noticeable, a similar up-and-down motion of the top line noted by the downward arrow can also be recognized by careful observation. To make such observations more clear, the bottom graph compares the peak and bottom intensities of the topographs. Lines of the mean intensity over each one fringe spacing are also given. Several fringes, not one, are related to these base- and top-line oscillations. In other words, intensity oscillation is demonstrated to occur also on a more global scale than the unit fringe spacing, besides the oscillation in individual fringes.

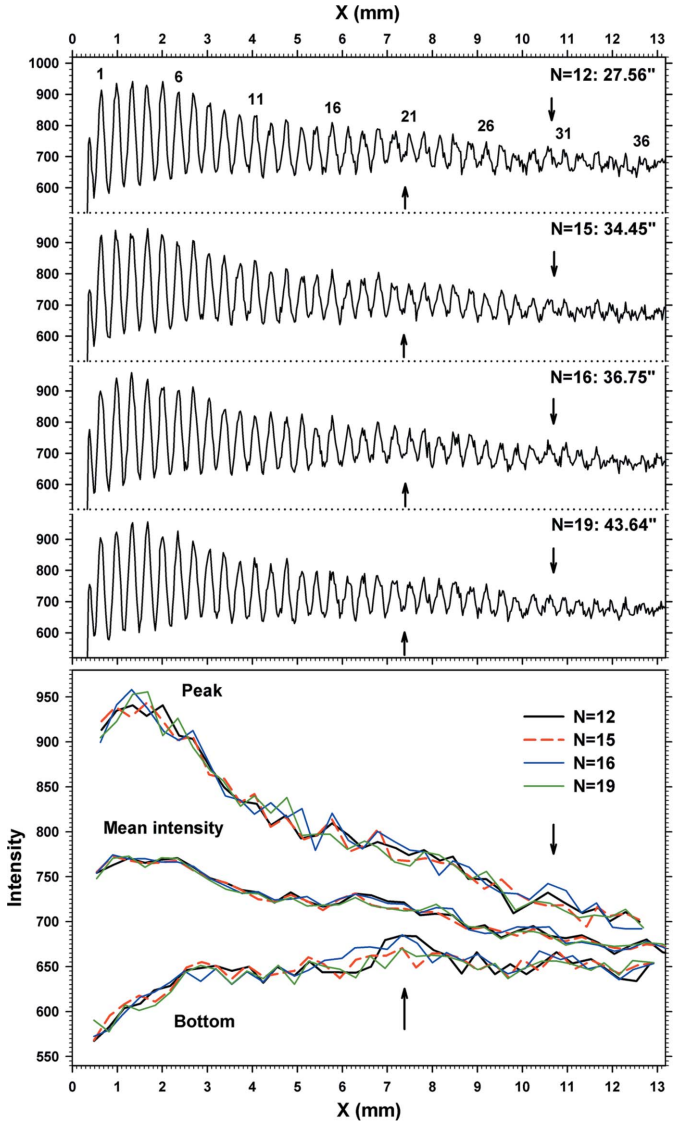

Figure 10
Intensity profiles (upper four graphs) of Pendellösung-fringe topographs viewed over a wide range to clarify global intensity oscillations (noted by arrow), and fringe-by-fringe plots (lowest graph) of the peak, bottom and mean intensities of fringes to be compared among topographs. The intensity profiles are measured in the same way as those in Fig. 4.

4. Discussion and conclusions

Observations and discussions in this paper are concluded with the following remarks.

(i) From the experiment using an X-ray CCD camera, a temporal oscillation of Pendellösung fringes has been observed for the first time. According to current knowledge (*e.g.* Kato, 1974), Pendellösung fringes are determined by the crystal thickness and lattice strain if any, as well as the wavelength, incidence angle and angular spread of the incident beam, and the lattice spacing and dielectric polarizability of the crystal. It is obvious that these determining factors did not change macroscopically during the imaging run, and therefore the observed fringe oscillation is not due to a change in them. Characteristics of the fringe oscillation viewed in fringe profiles, fringe-position plots and oscillation amplitude maps also support the idea that the fringe oscillation occurs as an intrinsic property of the fringes, and not caused by external force or conditions.

(ii) However, the claim for the observation of fringe oscillations had to be confronted with severe checks with regard to effects of the detector noise on data images. This is discussed in §3.1, §3.2.2 and §3.5.1. In conclusion, the observed fringe

oscillation and other fringe anomalies are basically real, although these observations and the quantitative estimation of the fringe oscillation would receive the influence of noise to some extent. As for the fringe profile change, experimental data approvable for the check of the $\pm 1.96\sigma_I$ error bar have to be presented in future. The accuracy of the quantitative fringe oscillation estimation has to be improved with reduction of noise effects.

(iii) The characteristics of the present temporal fringe oscillation are very similar to those of the previously observed spatial oscillation of moiré and Pendellösung fringes, as commented in this paper. Although the causes of these fringe oscillations are unknown, the oscillations cannot be unrelated since the apparent features resemble each other so much. Though not yet proven, it is natural to suppose that both oscillations have the same origin, showing different aspects of the same phenomenon.

(iv) Besides irregular fringe profiles and the fringe oscillation, the occurrence of subfringes and global intensity oscillation is also strange and is difficult to explain within the frame of existing knowledge. If this study can be continued, new strange fringe anomaly properties will further be disclosed. The mentioned anomalies are all supposed to be correlated with each another. The newly found anomalies above add clues to the origin of this fringe anomaly.

(v) For Pendellösung fringes of X-rays, much study has been carried out by precedent researchers. Wada & Kato (1977), for example, published an experimental observation of intensity profiles which are almost sinusoidal-shaped and in good agreement with theoretical calculation. The appearances of their Pendellösung fringes differ much from the presently described ones. However, the authors suppose that the two observations of Pendellösung fringes do not contradict each other in essence, and apparent differences would be due to differences in experimental conditions, such as the angular spread of the beam, differences in exposure time and in recording media (CCD camera or nuclear plates), and possibly differences in the beam coherence.

(vi) The intrinsic oscillation period of a temporal fringe oscillation, if it were so, would be much shorter than the time interval of 2.3 s in the present experiment. As faster observation is realised, the picture of this fringe oscillation is expected to be disclosed in a more essential form.

References

Kanamori, R., Iwamoto, T., Yoshimura, J., Hirano, K. & Zhang, X. (2000). *13th Annual Meeting of the Japanese Society for Synchrotron Radiation Research*, Abstract, p. 109. [In Japanese.]

Kato, N. (1974). *X-ray Diffraction*, ch. 3–5, edited by L. V. Azaroff, R. Kaplow, N. Kato, R. J. Weiss, A. J. C. Wilson and R. A. Young. New York: McGraw-Hill.

Wada, M. & Kato, N. (1977). *Acta Cryst.* A**33**, 161–168.

Yoshimura, J. (1989). *J. Phys. Soc. Jpn*, **58**, 1283–1295.

Yoshimura, J. (1991). *Acta Cryst.* A**47**, 139–141.

Yoshimura, J. (1993). *Study of Nonprojectiveness of X-ray Moiré-Fringed Images.* Report on research results to Grant-in-Aid for Scientific Research from The Ministry of Education and Science, Japan (No. 02452283). [In Japanese.]

Yoshimura, J. (1996). *Acta Cryst.* A**52**, 312–325.

Yoshimura, J. (2000). *J. Synchrotron Rad.* **7**, 374–381.

Yoshimura, J. (2004). *J. Synchrotron Rad.* **11**, 439–441.

Yoshimura, J., Hirano, K. & Zhang, X. (2001). *Photon Factory Activity Report*, #**18**, 187.